Intravital 2-photon imaging of leukocyte trafficking in beating heart

Wenjun Li,[1] Ruben G. Nava,[1] Alejandro C. Bribriesco,[1] Bernd H. Zinselmeyer,[2] Jessica H. Spahn,[1] Andrew E. Gelman,[1,3] Alexander S. Krupnick,[1] Mark J. Miller,[3] and Daniel Kreisel[1,3]

[1]Department of Surgery, Washington University School of Medicine, St. Louis, Missouri, USA. [2]NIH, National Institute of Neurological Disorders and Stroke, Bethesda, Maryland, USA. [3]Department of Pathology and Immunology, Washington University School of Medicine, St. Louis, Missouri, USA.

Two-photon intravital microscopy has substantially broadened our understanding of tissue- and organ-specific differences in the regulation of inflammatory responses. However, little is known about the dynamic regulation of leukocyte recruitment into inflamed heart tissue, largely due to technical difficulties inherent in imaging moving tissue. Here, we report a method for imaging beating murine hearts using intravital 2-photon microscopy. Using this method, we visualized neutrophil trafficking at baseline and during inflammation. Ischemia reperfusion injury induced by transplantation or transient coronary artery ligation led to recruitment of neutrophils to the heart, their extravasation from coronary veins, and infiltration of the myocardium where they formed large clusters. Grafting hearts containing mutant ICAM-1, a ligand important for neutrophil recruitment, reduced the crawling velocities of neutrophils within vessels, and markedly inhibited their extravasation. Similar impairment was seen with the inhibition of Mac-1, a receptor for ICAM-1. Blockade of LFA-1, another ICAM-1 receptor, prevented neutrophil adherence to endothelium and extravasation in heart grafts. As inflammatory responses in the heart are of great relevance to public health, this imaging approach holds promise for studying cardiac-specific mechanisms of leukocyte recruitment and identifying novel therapeutic targets for treating heart disease.

Introduction

Neutrophils play an important role in the defense against pathogens as well as in mediating sterile inflammation (1). A detailed understanding of the tissue-specific factors that regulate leukocyte recruitment to sites of inflammation is critical for the development of therapeutic strategies. Numerous studies have investigated interactions between neutrophils and endothelial cells in vitro (2). While such investigations have yielded valuable insight, observations made in vitro do not reliably model events in vivo, which may at least in part be due to differences in shear forces (3, 4). Moreover, there exist marked variations in the molecular requirements for neutrophil extravasation in vivo based on tissue environment and inflammatory stimuli (5). Site-specific differences in blood flow dynamics in different tissues and local patterns in the expression of adhesion molecules contribute to these variations.

Myocardial ischemia/reperfusion injury is a clinically relevant condition that occurs after restoration of blood flow following acute occlusion of coronary arteries as well as after heart transplantation. Experimental and clinical studies have demonstrated that neutrophils play a critical role in mediating tissue injury after myocardial ischemia/reperfusion (6). The intercellular adhesion molecule ICAM-1, a ligand for the β_2 integrins LFA-1 (CD11a/CD18) and Mac-1 (CD11b/CD18), plays an important role in the recruitment and extravasation of neutrophils to the site of injury (7). Two-photon (2P) microscopy has led to fundamental insights into the tissue-dependent behavior of leukocytes in response to inflammation in a variety of tissues. However, single-cell imaging within living heart tissue has not been considered feasible due to the rapid movement of the beating heart. We have now developed methods to image beating murine cardiac grafts in vivo. This report provides a detailed description of leukocyte trafficking within hearts during ischemia/reperfusion injury and demonstrates how this approach can be used to define the molecular requirements for leukocyte recruitment.

Results

Neutrophil imaging in resting and inflamed heart explants. We imaged neutrophil trafficking behavior in C57BL/6 (B6) LysM-GFP reporter mice in which neutrophils express high levels of GFP. Flow cytometric analysis of heart tissue 2 hours after transplantation into LysM-GFP recipient mice demonstrated that approximately 90% of the GFP^{hi} graft-infiltrating cells had high side scatter and expressed high levels of Gr1 and Ly6G, but not CD115, which is consistent with a neutrophil phenotype (Supplemental Figure 1; supplemental material available online with this article; doi:10.1172/JCI62970DS1). By 2P microscopy, neutrophils in LysM-GFP mice can be distinguished reliably from macrophages, which are dimmer and morphologically distinct (ref. 8 and Figure 1, A–C). To determine to what extent neutrophils entered heart tissue under steady state conditions, we imaged freshly explanted hearts derived from LysM-GFP mice. Blood vessels were visualized by injecting 12 μl of 655 nm nontargeted Q-dots in 50 μl of PBS intravenously prior to imaging. GFP-labeled cells and Q-dot–labeled blood vessels were excited by a Chameleon XR Titanium:Sapphire Laser (Coherent) tuned to 890 nm. Fluorescence emission was passed through 480-nm and 560-nm dichroic mirrors placed in series and detected as red (>560 nm), green (480 to 560 nm), and blue (<480 nm) channels by 3 head-on multialkali photomultiplier tubes. Each plane represents an image of 220 μm (x) by 240 μm (y) (at 2 pixels/μm). Z-Stacks were acquired by taking 21 sequential steps at 2.5-μm spacing. 2P microscopy revealed

Authorship note: Wenjun Li, Ruben G. Nava, and Alejandro C. Bribriesco share first authorship. Mark J. Miller and Daniel Kreisel share senior authorship.

Conflict of interest: The authors have declared that no conflict of interest exists.

Citation for this article: *J Clin Invest.* 2012;122(7):2499–2508. doi:10.1172/JCI62970.

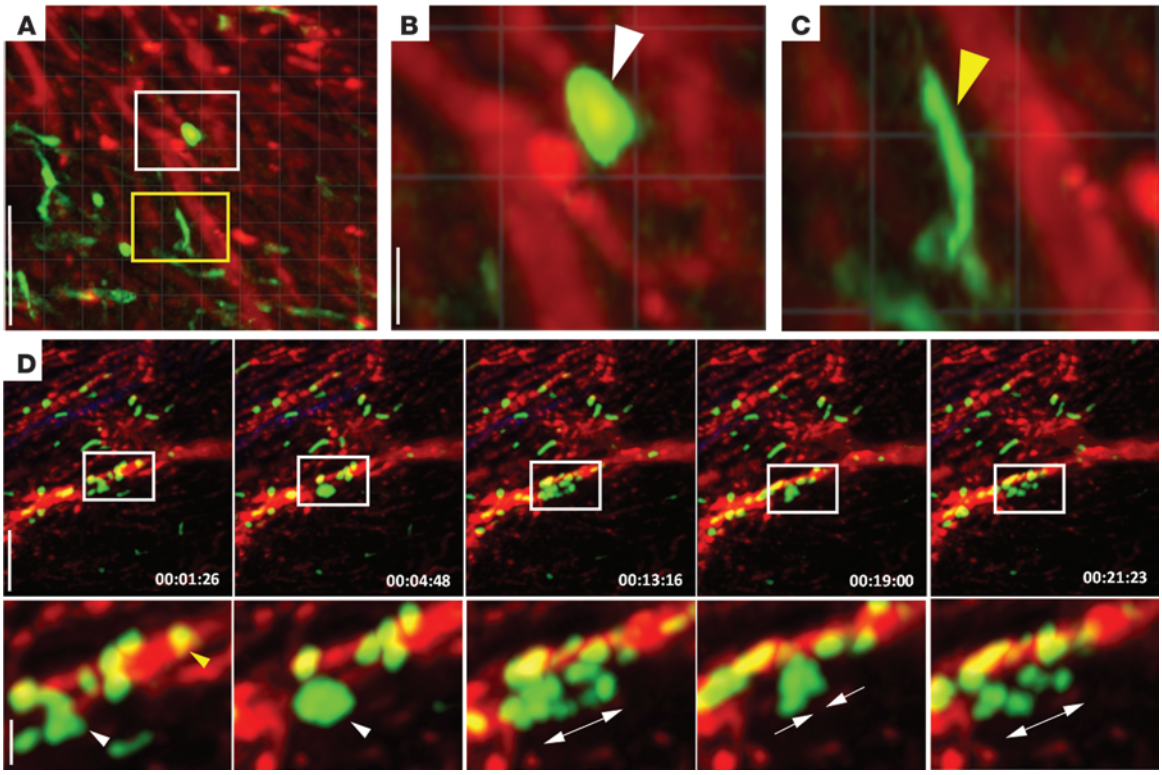

Figure 1
2P microscopy of neutrophils in explanted heart at steady state and after heterotopic heart transplantation. (**A**) Myocardial tissue with resident neutrophils (green cells, white box) and macrophages (green cells, yellow box). Nontargeted Q-dots were injected intravenously 10 minutes before imaging to label the blood vessels (red). Scale bar: 60 μm. (**B** and **C**) Zoomed views from panel **A** showing (**B**) an intravascular neutrophil (white arrowhead) and (**C**) a macrophage (yellow arrowhead). These cells can be distinguished by morphology and fluorescence intensity. Scale bar: 10 μm. (**D**) Time-lapse images of neutrophils in explanted heart tissue after heterotopic cardiac transplantation into B6 LysM-GFP mice. Images are individual frames from a continuous time-lapse recording (Supplemental Video 1). Relative time is displayed in h:min:s. Lower panels are zoomed views from the boxed regions. Neutrophils were found adhering to the endothelium (yellow arrowhead) or crawling along it. Extravascular neutrophils (white arrowheads) formed dynamic clusters (white arrows) over minutes. Scale bars: 60 μm (upper panels); 20 μm (lower panels). Data are representative of at least 3 independent experiments per group.

that only rare neutrophils were visible in the heart at baseline, and these cells were found nearly exclusively within small capillaries. We did not find any evidence of neutrophil adhesion or extravasation in 3 independent experiments (Figure 1A). We next assessed neutrophil responses under inflammatory conditions using a model of ischemia/reperfusion injury after heterotopic heart transplantation. We examined neutrophil recruitment in explanted B6 cardiac grafts 3 hours after transplantation into syngeneic LysM-GFP mice (Figure 1D). Many neutrophils were found arrested on the endothelium within coronary veins. As shown in 2P time-lapse videos, neutrophils crawled along the endothelium and then extravasated from vessels into the myocardium, where they aggregated in dynamic clusters of 8–10 cells (Supplemental Video 1). Neutrophil clusters developed and disassociated over several minutes (Figure 1D). When cardiac explants were imaged at 6 hours after reperfusion, neutrophil clusters within the myocardium increased in frequency and size (Supplemental Figure 2). Although laser-induced damage can cause neutrophil clustering, we took care to keep the photomultiplier gain as high as possible and use only enough laser as required to detect the cells. Furthermore, because our 2P microscope employs resonant scanning, the laser dwell time and hence damage is highest at the edges of the images. The absence of visible thermal damage to the tissue and the fact that the clusters are more centrally located suggest that neutrophil clustering is not an artifact of laser damage.

In vivo neutrophil recruitment dynamics in heart grafts during inflammation. Due to the lack of blood flow and absence of contractions, neutrophil behavior in cardiac explants may not accurately reflect conditions in vivo. In particular, neutrophil rolling, firm adhesion, and extravasation are likely to be influenced by vessel flow characteristics as well as the mechanical force transmitted to vessels by the heartbeat. Therefore, we developed a 2P intravital imaging approach to study leukocyte recruitment behavior within beating transplanted hearts (Figure 2). Briefly, B6 WT hearts were transplanted into the neck of syngeneic LysM-GFP mice and imaged one hour after reperfusion. The neck incision was reopened to expose the heart graft. A portion of the free wall of the left ventricle of the transplanted heart was secured using a thin ring of Vetbond tissue adhesive applied to a glass coverslip attached to the upper chamber plate. Due to the superficial location of the transplanted heart, the graft was partially exteriorized during imaging. Because the heart is imaged close to the cover glass and the cardiac tissue moves away

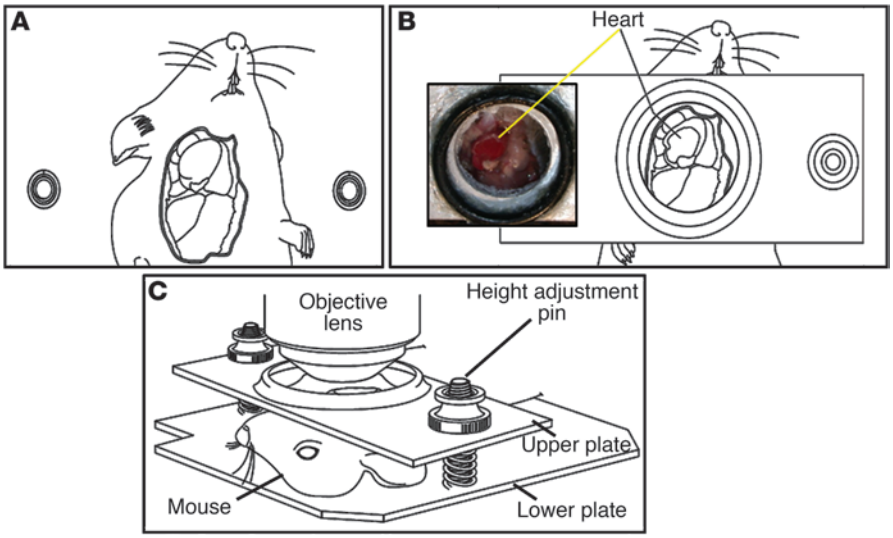

Figure 2
2P microscopy of heterotopic heart transplants. (**A**) Depiction of an exposed heterotopic transplanted heart in the right cervical region with mouse placed on the base plate of the imaging chamber. (**B**) A small ring of Vetbond is applied to the bottom of the coverglass portion of the stabilization plate and briefly held against the heart to secure the tissue. The upper plate is adjusted to minimize pressure on the heart. (**B**, inset) Photograph of in vivo preparation with affixed heart graft indicated by yellow line. (**C**) Side view of the imaging set up showing the mouse, the upper and bottom chamber plates, and the microscope objective.

from the cover glass as the heart beats, motion artifacts were minimal during imaging at depths of up to 120 μm. To further reduce tissue motion, an effort was made to synchronize the Z-Stack acquisition with the heartbeat. Therefore, videos of superficial structures such as coronary veins are very stable, and the cells are easily tracked. Imaging was feasible up to depths of approximately 220 μm. However, contractions were more evident when structures that lie deeper within the heart, such as coronary arterial branches, were imaged. Neutrophils were seen flowing through coronary arteries, but we did not observe prolonged interactions between neutrophils and arterial endothelium (Figure 3 and Supplemental Video 2). Unlike other tissues, in which neutrophils adhere to and extravasate from postcapillary venules, in reperfused hearts, the majority of neutrophils adhered to the walls of larger coronary veins (Figure 4A and Supplemental Video 3). The intravascular rolling velocity for neutrophils in coronary veins was 145.9 ± 50.3 μm/s (Figure 4E). After adhesion, neutrophils displayed intraluminal crawling (average velocity of 8.79 ± 11.4 μm/min) (Figure 4F) and congregated in intravascular clusters (9.6 ± 3.05 clusters in a representative 220- by 240-μm area) (Figure 4G) with an average of 8.4 ± 2.1 neutrophils in each cluster (Figure 4H).

ICAM-1 and its ligands LFA-1 and Mac-1 are important mediators of neutrophil recruitment. We examined the role of ICAM-1 in neutrophil trafficking during transplant-mediated ischemia/reperfusion injury in the heart. B6 ICAM-1–mutant hearts, in which a neomycin resistance gene had been inserted into exon 4 of the *Icam1* gene, were transplanted into syngeneic LysM-GFP recipients, and intravital 2P microscopy was initiated 1 hour after reperfusion. In these ICAM-1–mutant hearts, neutrophils were arrested along the endothelial wall of coronary veins forming large clusters (Figure 4B and Supplemental Video 4). In ICAM-1–mutant cardiac grafts, we observed a significant reduction in both intravascular rolling (94.34 ± 37.36 vs. 145.9 ± 50.3 μm/min; $P < 0.01$) (Figure 4E) and crawling velocities (4.33 ± 3.31 vs. 8.79 ± 11.4 μm/min, $P < 0.01$) (Figure 4F) of neutrophils. In addition, there was a trend toward a greater number of neutrophil clusters in ICAM-1–mutant hearts compared with WT grafts (18 ± 4.5 vs. 9.6 ± 3.05; $P = 0.05$) (Figure 4G), and the number of neutrophils per cluster was significantly higher in ICAM-1–mutant than in WT hearts (15.23 ± 1.13 vs. 8.4 ± 2.1; $P < 0.01$) (Figure 4H). Furthermore, unlike clusters in WT hearts, which appeared well circumscribed, neutrophils were spread over larger surface areas in the vessels of ICAM-1–mutant grafts (Figure 4, A and B). When we treated cardiac transplant recipients with LFA-1–blocking antibodies, neutrophils interacted with the vessel wall and rolled at velocities comparable to those of untreated mice (137.3 ± 59.1 vs. 145.9 ± 50.3 μm/min; $P = 0.47$) (Figures 4, C and E, and Supplemental Video 5). However, the vast majority of neutrophils did not slow down enough to transition to adherence and crawling. Consequently, the number of neutrophil clusters (Figure 4G) was significantly lower after LFA-1 blockade than in untreated recipients of WT (3.33 ± 0.5 vs. 9.66 ± 3.05; $P = 0.02$) or ICAM-1–mutant hearts (3.33 ± 0.5 vs. 18 ± 4.5; $P < 0.01$). Also, the number of neutrophils per cluster was significantly lower after treatment with LFA-1–blocking antibodies when compared with those of untreated heart recipients (2.51 ± 0.41 vs. 8.42 ± 2.1; $P < 0.01$) or recipients of ICAM-1–mutant grafts (2.51 ± 0.41 vs. 15.23 ± 1.13; $P < 0.01$) (Figure 4H). Intravascular neutrophil behavior after blockade of Mac-1 (Figure 4D and Supplemental Video 6) was comparable to that seen in ICAM-1–mutant cardiac grafts (Figure 4B).

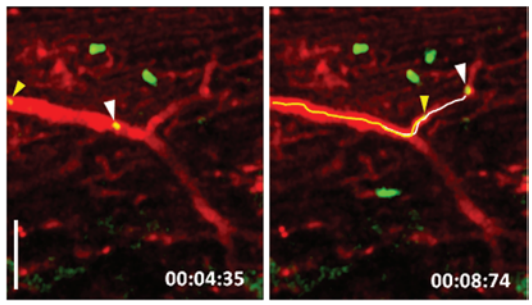

Figure 3
Coronary artery imaging in vivo. (Supplemental Video 2) Video rate images show individual neutrophils (yellow and white arrowheads) moving (yellow and white tracks) in a coronary artery labeled with Q-dots (red). Other neutrophils are visible in nearby capillaries. Relative times are displayed in min:s:ms. Scale bar: 60 μm.

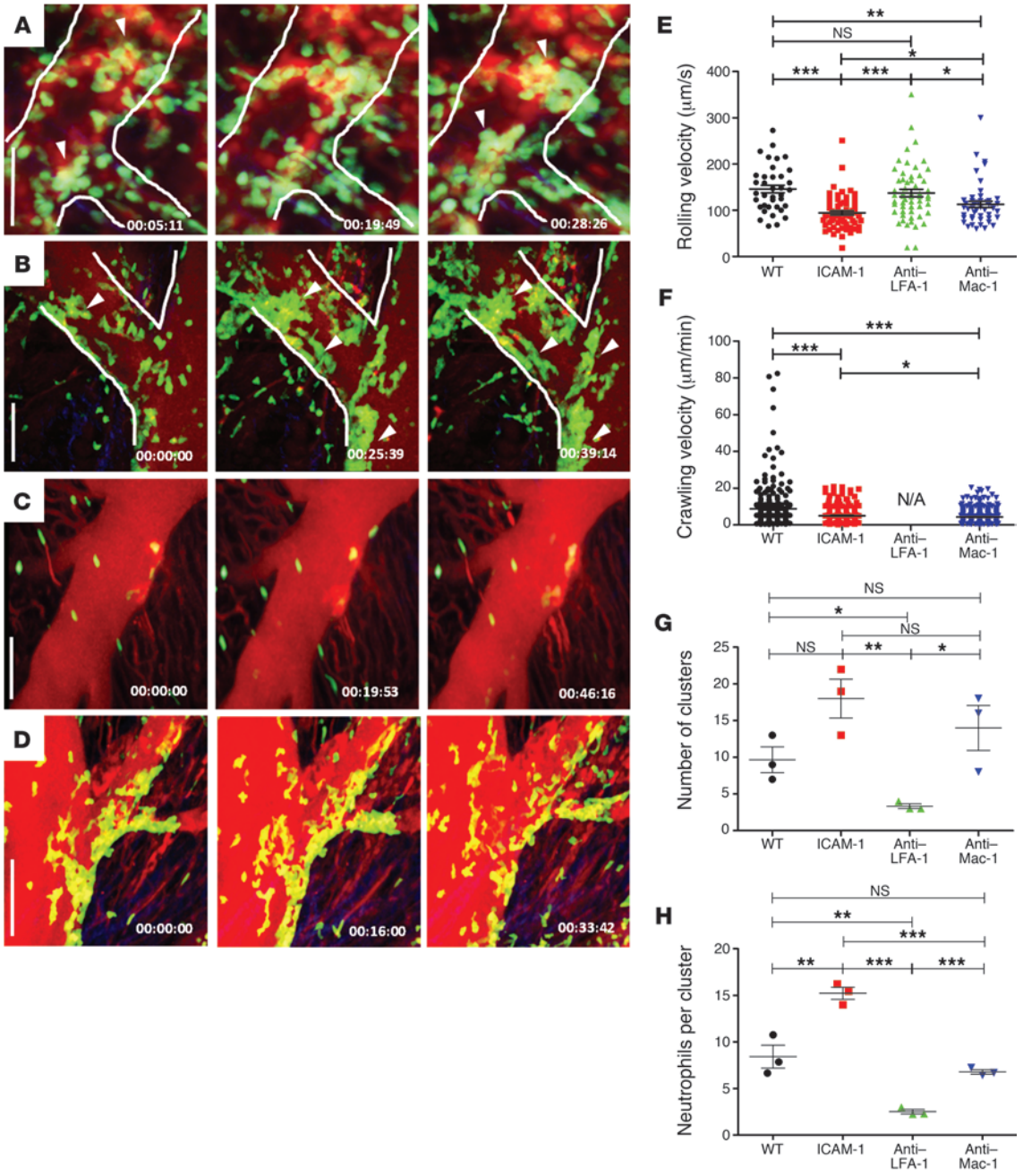

Figure 4

2P imaging of intravascular neutrophil dynamics in heterotopic heart transplants. (**A**, Supplemental Video 3) WT heart graft with extensive neutrophil arrest inside blood vessels (white outline) and intravascular cluster formation (white arrowheads). $n = 4$ mice. Comparable results were obtained in untreated and isotype control–treated recipients of WT cardiac grafts. (**B**, Supplemental Video 4) Neutrophil trafficking in ICAM-1–mutant (denoted as ICAM-1) donor hearts ($n = 2$ mice), (**C**, Supplemental Video 5) after treatment of recipient mice with anti-LFA 1 ($n = 4$ mice), and (**D**, Supplemental Video 6) after treatment with anti-Mac 1 antibodies ($n = 4$ mice). Scale bars: 60 μm. (**E**) A comparison of cell-rolling velocities in each group. Rolling velocities were lower in ICAM-1–mutant grafts and anti–Mac-1–treated recipient mice compared with WT mice, while velocities after treatment with anti–LFA-1 were comparable to those in WT. WT, $n = 37$; ICAM-1–mutant, $n = 61$; anti–LFA-1, $n = 56$; anti–Mac-1, $n = 47$. $^{*}P < 0.05$; $^{**}P < 0.01$; $^{***}P < 0.0001$. (**F**) Intraluminal crawling velocities. ICAM-1–mutant grafts, and anti–Mac-1–treated recipients had significantly lower crawling velocities when compared with WT mice. Due to the low number of adherent neutrophils, crawling activity could not be analyzed after blockade of LFA-1. WT, $n = 260$; ICAM-1–mutant, $n = 317$; anti–LFA-1, n = NA; anti–Mac-1, $n = 481$. $^{*}P < 0.05$; $^{***}P < 0.0001$. For parts **E** and **F**, symbols represent individual cells, and horizontal bars depict means. (**G**) Intravascular neutrophil clusters. Cluster frequency increased in ICAM-1–mutant hearts and with anti–Mac-1 antibody treatment and decreased when LFA-1 was blocked. $^{*}P < 0.05$; $^{**}P < 0.01$. Symbols represent intravascular neutrophil clusters. (**H**) Neutrophil cluster size. ICAM-1–mutant grafts had larger neutrophil clusters compared with WT hearts. $^{**}P < 0.01$; $^{***}P < 0.0001$. For **G** and **H**, horizontal bars denote means, and error bars denote SEM.

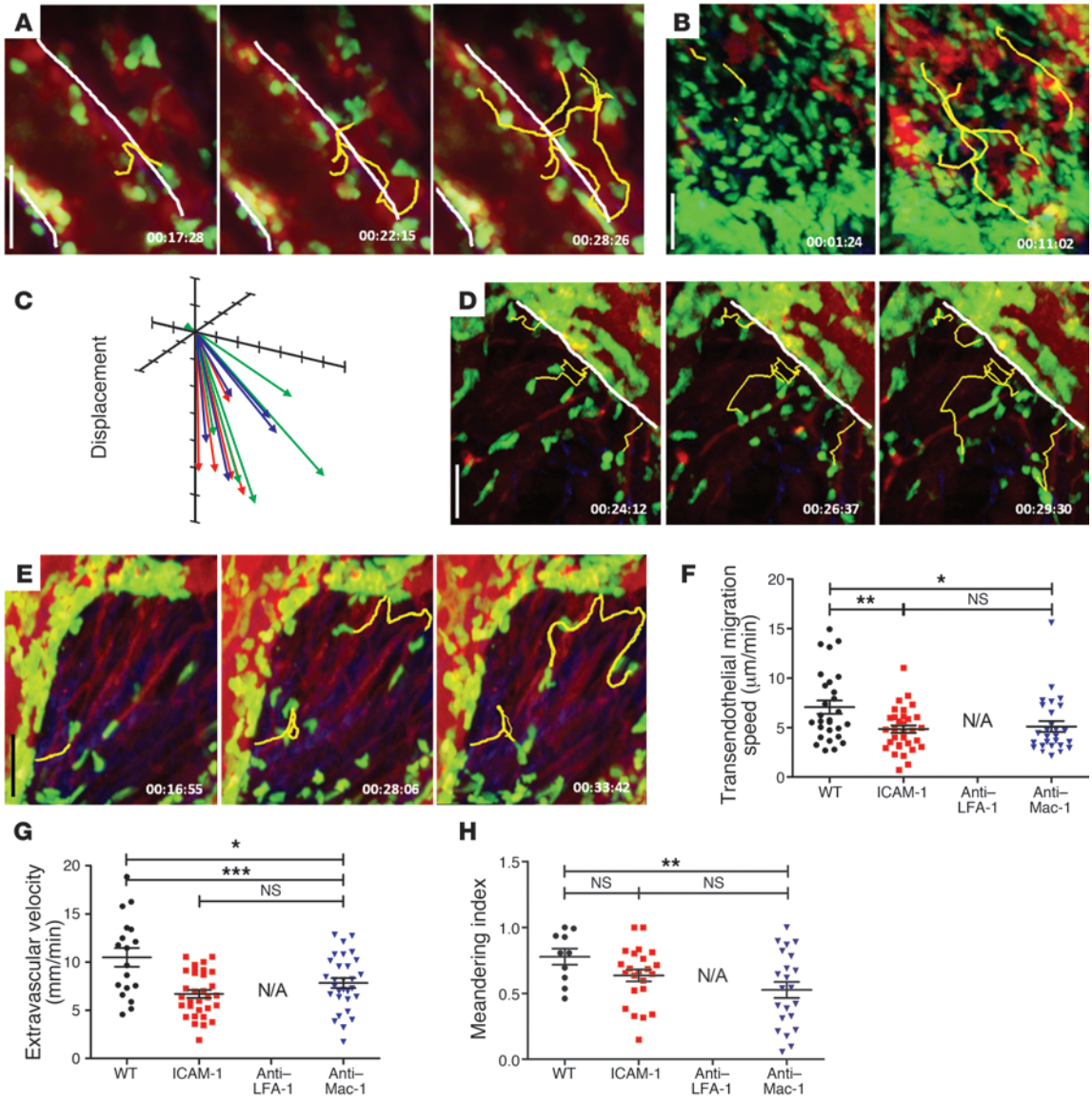

Figure 5

Extravascular neutrophil trafficking. (**A**, Supplemental Video 3) Time-lapse images of WT heart grafts showing individual neutrophils extravasating (yellow tracks) and migrating through cardiac tissue with mean speeds of 10.48 ± 4.1 μm/min (n = 4 mice). (**B**) Large extravascular clusters of neutrophils in the ventricular wall of WT grafts. Individual neutrophils migrate toward dynamic clusters (yellow tracks). (**C**) Direction of neutrophil displacement in B6 WT hearts after transplantation into syngeneic LysM-GFP mouse (n = 18). (**D** and **E**) Time-lapse imaging of neutrophil extravasation in (**D**, Supplemental Video 4) ICAM-1–mutant grafts (n = 2 mice) and (**E**, Supplemental Video 5) after Mac-1 blockade of heart transplant recipients (n = 4 mice). Scale bars: 60 μm. (**F**) Speed of transendothelial migration from luminal surface to tissue parenchyma (WT, n = 28; ICAM-1–mutant, n = 32; anti–LFA-1, n = NA; anti–Mac-1, n = 27; $^*P < 0.05$; $^{**}P < 0.01$), (**G**) velocity (WT, n = 18; ICAM-1–mutant, n = 31; anti–LFA-1, n = NA; anti–Mac-1, n = 30; $^*P < 0.05$; $^{***}P = 0.0002$) and (**H**) meandering indices (WT, n = 10; ICAM-1–mutant, n = 23; anti–LFA-1, n = NA, anti–Mac-1, n = 22; $^{**}P < 0.01$) of extravasated neutrophils in experimental groups. Symbols represent individual cells, and horizontal bars depict means. Virtually no neutrophils extravasated after blockade of LFA-1. Relative times are displayed in h:min:s for all images.

Neutrophils rolled along the walls of coronary veins and arrested along the endothelium in clusters (Figure 4D). The intravascular neutrophil clusters observed in anti–Mac-1 antibody–treated mice resembled morphologically those seen in ICAM-1–mutant hearts. After blockade of Mac-1, neutrophil rolling velocity was reduced compared with that in untreated controls (112.9 ± 45.96 vs. 145.9 ± 50.3 μm/min; $P < 0.01$) and recipients that received anti–LFA-1 antibodies (112.9 ± 45.96 vs. 137.3 ± 59.1; $P = 0.02$), but was higher than that observed in ICAM-1–mutant grafts (112.9 ± 45.96 vs. 94.34 ± 37.36; $P = 0.02$) (Figure 4E). Finally, blocking Mac-1 reduced intravascular crawling velocities to significantly lower levels than those in untreated controls (4.33 ± 3.31 vs. 8.79 ± 11.4 μm/min; $P < 0.01$) and ICAM-1–mutant grafts (4.33 ± 3.31 vs. 4.98 ± 3.86 μm/min; $P < 0.05$) (Figure 4F). However, the number of clusters did not differ significantly compared with those in untreated WT (14 ± 5.29 vs. 9.6 ± 3; $P = 0.28$) or ICAM-1–mutant

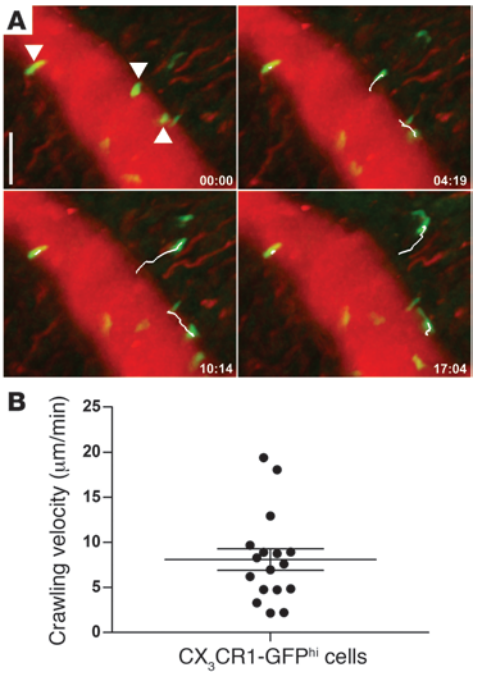

Figure 6
Intravital 2P imaging of CX_3CR1-GFP^{hi} cells in heterotopic heart transplants. (**A**) Time-lapse images of WT heart grafts showing individual CX_3CR1-GFP^{hi} cells crawling, extravasating, and migrating through myocardial tissue (marked with white arrowheads and white tracks). *n* = 3 mice. Relative times are displayed in min:s for all images. Scale bar: 60 μm. (**B**) Intraluminal crawling velocity of CX_3CR1-GFP^{hi} cells. *n* = 17 cells. Symbols represent individual cells, horizontal bars depict means, and error bars represent SEM.

hearts (14 ± 5.29 vs. 18 ± 4.5; $P = 0.37$), but it was significantly higher when compared with those of animals that received treatment with anti–LFA-1 antibodies (14 ± 5.29 vs. 3.33 ± 0.5; $P = 0.02$) (Figure 4G). The number of cells per cluster was comparable to that of untreated controls (6.79 ± 0.41 vs. 8.42 ± 2.1; $P = 0.25$), significantly lower when compared with ICAM-1–mutant hearts (6.79 ± 0.41 vs. 15.23 ± 1.13; $P < 0.01$), and higher than after LFA-1 blockade (6.79 ± 0.41 vs. 2.51 ± 0.41; $P < 0.01$) (Figure 4H).

Neutrophil extravasation in heart grafts during inflammation. In untreated heart recipients, neutrophils left the coronary veins and entered the myocardial tissue. Extravasation occurred at specific sites, where neutrophils were seen entering the tissue in single-file fashion (Figure 5 and Supplemental Video 3). The speed of transendothelial migration was significantly reduced in ICAM-1–mutant grafts or when Mac-1 was blocked with antibody (Figure 5F). Extravasated neutrophils migrated through the myocardium with a velocity of 10.48 ± 4.12 μm/min (Figure 5G) and formed large dynamic clusters (Figure 5B). Neutrophil infiltration into the myocardial tissue increased over time, and by 24 hours after reperfusion, we observed a marked increase in neutrophil cluster size (Supplemental Figure 3 and Supplemental Video 7). Cell displacement was predominately unidirectional (Figure 5C), and neutrophils moving toward clusters displayed a meandering index (MI = 0.81) consistent with chemotactic behavior (Figure 5H). In ICAM-1–mutant hearts, neutrophil extravasation occurred infrequently (Figure 5D) and extravasated neutrophils migrated with significantly decreased velocities (6.69 ± 2.32 vs. 10.48 ± 4.12 μm/min; $P < 0.01$) (Figure 5G) and displayed nearly random paths, as evidenced by an MI of 0.6 ± 0.24 (Figure 5H). In contrast, virtually no neutrophils entered the myocardial tissue when LFA-1 was blocked. Similarly to ICAM-1–mutant hearts, neutrophils in anti–Mac-1–treated heart recipients left the circulation in reduced numbers (Figure 5E) and displayed decreased velocities (7.83 ± 2.84 μm/min) and more random paths (MI = 0.52 ± 0.26) within the myocardial tissue (Figures 5, F and G).

Trafficking of CX_3CR1^+ cells in heart grafts. To extend our approach to other leukocyte types beyond neutrophils, we assessed cell recruitment into reperfused cardiac grafts by using CX_3CR1 GFP/+ reporter mice as heart transplant recipients. These mice express GFP in monocytes as well as in a small fraction of NK cells, but not in neutrophils (9). Within 1 hour of reperfusion CX_3CR1 GFP^{hi} cells were present within the transplanted hearts. Similar to neutrophils, CX_3CR1 GFP^{hi} cells interacted with the endothelium of larger coronary veins, displaying rolling, adhesion, and intraluminal crawling behaviors (Figure 6A and Supplemental Video 8). CX_3CR1 GFP^{hi} cells crawled at 8.1 ± 1.2 μm/min (Figure 6B) and in some cases against the direction of the blood flow. Extravasated cells migrated through the myocardial tissue without aggregating into clusters, in contrast to neutrophil behavior.

Neutrophil trafficking in native hearts. We next set out to image native hearts in their anatomic position. Native hearts were exposed through a left anterior thoracostomy, where portions of the second through fifth ribs were resected. Attention needed to be directed toward avoiding injury to the left internal mammary artery. Following removal of the pericardial sac, a small ring of Vetbond was used to attach a portion of the free wall of the left ventricle to the bottom of the cover glass. Removal of the pericardium did not induce detectable inflammatory changes in the heart tissue (Supplemental Figure 4). Our imaging preparation exerted virtually no direct pressure on the heart tissue and therefore was well tolerated by mice for up to 3 hours. During imaging, mice maintained a steady heart rhythm and the peripheral tissues looked pink and well perfused. Occasionally, neutrophils were seen flowing rapidly through arterial vessels at velocities approaching 2000 μm/s (Figure 7A and Supplemental Video 9). Under baseline conditions, only a few neutrophils resided in the heart tissue (Figure 7B). We did not observe neutrophil rolling or crawling behaviors in the absence of inflammation. However, transient ligation of the left main coronary artery for 30 minutes induced the rapid recruitment of neutrophils to coronary blood vessels apparent as both rolling at 116.1 ± 39.8 μm/s (Figure 7, C and D) and crawling behaviors at 14.5 ± 3 μm/min (Figure 7, E and F). Furthermore, compared with unmanipulated hearts, a larger number of extravascular neutrophils were detected in the myocardial tissue, some of which aggregated into clusters (Figure 7G and Supplemental Video 10).

Discussion

Our understanding of the pathogenesis of cardiovascular diseases has been aided by the development of various technologies for imaging murine hearts, such as computed tomography, magnetic resonance imaging, and ultrasound. Especially in combination with molecular probes, such approaches have provided important insight into atherosclerotic plaque behavior, myocardial viability, and engraftment of stem cells (10). However, our understanding of the dynamic behavior of leukocytes

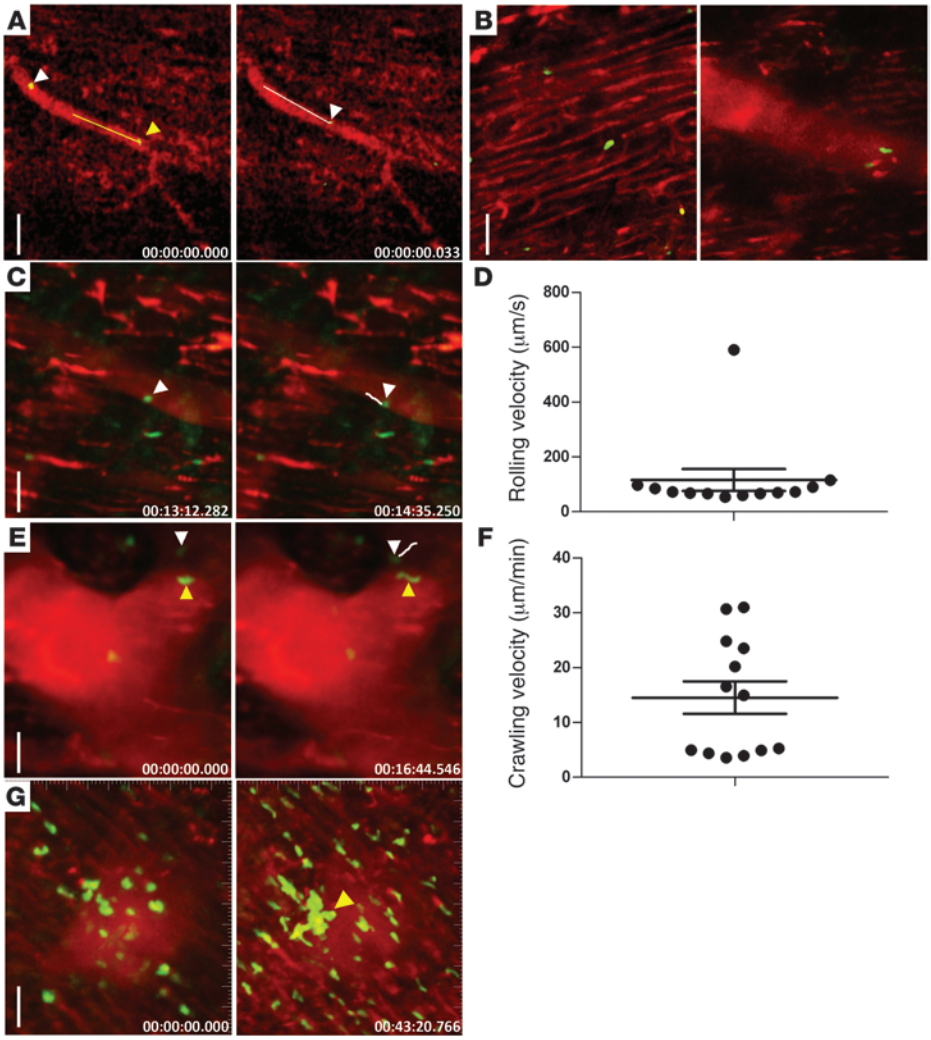

Figure 7
Intravital 2P imaging of the native murine heart. B6 LysM-GFP hearts were imaged in their natural intrathoracic position. All mice tolerated imaging for at least 1 hour, with the majority of imaging periods lasting more than 3 hours. (**A**, Supplemental Video 9) Sequential video-rate frames of 2 neutrophils (yellow arrowhead with yellow track and white arrowhead with white track) moving through a coronary artery. The measured speed of the neutrophil marked in yellow is 1875.2 μm/s. (**B**) Representative images of native hearts in the steady state depicting capillaries (red, left panel) and a vein (red, right panel). Only few neutrophils (green) are visible. (**C**, **E**, **G**) 2P microscopy of beating native hearts after ischemia/reperfusion induced through transient ligation of the left coronary artery. (**C**) Intravascular rolling behavior of neutrophils (white arrowheads) was observed in coronary veins (white track). (**D**) Analysis of rolling velocities in native hearts subjected to ischemia/reperfusion injury. (**E**) Crawling behavior (yellow arrowhead) was associated with cell flattening along the endothelium. A second crawling neutrophil is indicated by a white arrowhead and white track. (**F**) Analysis of crawling velocities in native hearts subjected to ischemia/reperfusion injury. Symbols represent individual cells, horizontal bars depict mean, and error bars represent SEM. (**G**, Supplemental Video 10) Dynamic neutrophil clusters (yellow arrowheads) in myocardial tissue of native hearts that have been subjected to ischemia/reperfusion injury. Blood vessels (red) were labeled by intravenous injection of nontargeted 655-nm Q-dots. Relative time is displayed in h:min:s. Scale bars: 60 μm. Data are representative of 4 independent experiments.

in hearts at steady state and during inflammation is poor. Myocardial ischemia/reperfusion injury is a morbid condition that can result in ultrastructural damage and adversely affect heart function acutely as well as chronically. Common clinical scenarios in which ischemic myocardium is reperfused include heart transplantation and restoration of blood flow after blockage of coronary arteries through interventions such as thrombolysis, angioplasty, or surgical bypass. Clearly, a detailed understanding of the mechanisms that contribute to myocardial ischemia/reperfusion injury will lead to the development of new therapeutic approaches. In the current study, we developed a method to image both beating murine cardiac grafts and native hearts by intravital 2P microscopy. Moreover, we analyzed neutrophil recruitment in real time during inflammation using a clinically relevant model. We showed that our imaging approach could be used to determine precisely how antibody-mediated integrin blockade affects neutrophil behavior within coronary vessels and the myocardial tissue.

Because intravital 2P microscopy captures single-cell dynamics in vivo, this approach often provides unique insights for understanding how innate and adaptive immune responses are regulated. Compared with other techniques, 2P imaging has the advantages of increased tissue viability, reduced photobleaching, and deep tissue penetration (11). 2P microscopy has become increasingly popular with immunologists since it was first used to image explanted tissues and later extended to image a wide variety of lymphoid and nonlymphoid tissues in vivo, including lymph nodes, spleen, kidneys, and brain (12). Intrathoracic organs that are subject to motion have not been considered amenable to intravital 2P microscopy. To address these technical hurdles, our group and others have recently developed methods to stabilize murine lungs within the thoracic cavity, which allowed for the study of neutrophil dynamics in lungs at baseline and during inflammation (8, 13). Notably, we observed that tissue-resident neutrophils behaved differently in explanted lungs compared with live lungs, raising the possibility that surgical removal of organs prior to imaging may alter cellular behavior (8). In the current study, we have adapted the methods that have allowed us to image lungs to the beating heart. Due to concerns that mice would not tolerate stabilization of their native hearts, we initially imaged heterotopic cardiac transplants. This model is commonly used by immunologists to study ischemia/reperfusion injury and acute and chronic rejection (14). While the coronary circulation is perfused and these heterotopic heart grafts are beating, they do not contribute to the hemodynamics of the recipient. As we gained experience with intravital imaging of cardiac grafts, we were able to adapt our techniques to image native beating hearts. Surprisingly, this procedure was well tolerated by mice for up to 3 hours without loss of tissue perfusion.

In this study, we have focused on neutrophils because of their well-established role in mediating sterile inflammation. To this end, canine studies have demonstrated that neutrophil depletion reduces myocardial ischemia/reperfusion injury (15, 16). In contrast to our recent observations for resting lungs, virtually no neutrophils reside in the myocardial tissue under resting conditions (8). Neutrophils, however, rapidly infiltrate ischemic hearts following reperfusion. Unlike the case for other tissues and organs in which neutrophils exit from postcapillary venules, in the heart, neutrophils leave the circulation from larger coronary veins. Recruitment of neutrophils into inflamed tissues is a tightly regulated multistep process. In the coronary vessels, neutrophils roll along the endothelium, adhere, and undergo intraluminal crawling and then extravasation. Neutrophils can crawl with and against the blood flow to reach extravasation sites on the endothelium. Previous studies have shown that neutrophils aggregate with platelets, which promotes the activation of neutrophils and their recruitment into inflamed tissues (17, 18). We speculate that the neutrophil clusters that form within coronary veins are likely sites of thrombosis. To this end, platelet aggregates may provide a scaffold that allows neutrophils to tether to sites of activated endothelium before they extravasate. Importantly, in vitro flow chamber systems may not accurately model events in vivo, and organ-specific differences in leukocyte recruitment are well recognized. For example, while ICAM-1 on endothelial cells is critical for neutrophil adhesion in cremasteric postcapillary venules, neutrophils can adhere to hepatic sinusoids independently of ICAM-1 (19, 20). ICAM-1 is upregulated on endothelial cells of coronary vessels following ischemia, which is in large part due to the release of proinflammatory cytokines such as TNF-α (21, 22). Blocking ICAM-1 has been shown to ameliorate myocardial ischemia/reperfusion injury in rodent models of heart transplantation and transient ligation of a coronary artery (23, 24). The ICAM-1–mutant strain used in this study is not completely devoid of ICAM-1 expression, but rather expresses alternatively spliced isoforms that lack an Ig-like domain, which is the binding site for Mac-1. Although WT recipient neutrophils were able to adhere to the endothelium of ICAM-1–mutant grafts, the intravascular clusters were spread out over a larger surface; this is similar to our observations after Mac-1 blockade. This could in large part be due to a deficiency in neutrophil crawling when ICAM-1 or Mac-1 are inhibited, consistent with a previous study in a cremaster muscle preparation (25). While impaired crawling in ICAM-1–mutant hearts is likely to contribute to the low rate of neutrophil extravasation, ICAM-1 may also play a role further downstream during their transendothelial migration (26, 27). Others have suggested that when crawling is impaired, leukocytes use a transcellular rather than a paracellular path to enter the tissue. Our in vivo model does not allow us to make definitive statements about the route of transendothelial migration, since the endothelium is not directly visualized. However, we consistently observed that neutrophils extravasated at "hot spots" in both WT and integrin signaling–blocked mice, suggesting that paracellular migration is the likely mechanism. Moreover, we were able to show that extravasation at these sites was less efficient when ICAM-1 was mutated or Mac-1 was inhibited, revealing that these molecules may play a role during transendothelial migration in addition to intraluminal crawling. However, neutrophil emigration into injured myocardial tissue was not completely abrogated when donor hearts expressed alternatively spliced ICAM-1. Previous studies have shown that, in addition to ICAM-1, VCAM-1, an adhesion molecule that interacts with β_1 integrins on leukocytes, is upregulated on cardiac endothelium during ischemia/reperfusion injury (28). Furthermore, in hearts, VCAM-1 plays an important role in promoting the transendothelial migration of neutrophils that lack expression of CD18 and therefore cannot interact with ICAM-1 (28). The possibility exists that VCAM-1 may mediate some degree of neutrophil infiltration into heart grafts that express alternatively spliced ICAM-1 or in the absence of Mac-1 interactions.

In contrast to our findings, other investigators have reported that inhibition of Mac-1 results in increased emigration of neutrophils when employing a model of TNF-α–mediated leukocyte extravasation in a subcutaneous air pouch model (29). It has also been suggested that Mac-1 may inhibit the migration of neutrophils in the interstitium following their transendothelial migration. We observed slower movement and random migration of extravasated neutrophils after inhibition of Mac-1 or within ICAM-1–mutant myocardial tissue. As myocytes within ischemic hearts express ICAM-1 (30), our findings support the notion that ICAM-1 expression on cardiomyocytes regulates neutrophil behavior within reperfused hearts. In addition, ICAM-1 expression on cardiomyocytes may regulate the function of neutrophils, as suggested by in vitro canine studies demonstrating that neutrophil adhesion to myocytes and their oxidative burst can be inhibited by blocking ICAM-1 or Mac-1 (31).

Notably, neutrophil adherence in coronary veins was virtually absent when LFA-1 was blocked. Consequently, we could not delineate a role for LFA-1 in crawling, extravasation, or migration within inflamed myocardial tissue. In other tissues, such as cremasteric muscle, where some neutrophils adhere when LFA-1 is inhibited, LFA-1 blockade does not have an impact on their behavior following adherence (25). Rolling velocities of neutrophils in coronary veins are approximately 3-fold higher than those observed in cremasteric vessels, which may in part be due to differences in vessel diameter. Previous studies have indicated that rolling velocities of neutrophils are increased in inflamed mesenteric or cremasteric vessels in the absence of LFA-1 (25, 32, 33). In contrast, we observed that blockade of LFA-1 did not affect rolling velocities of neutrophils in the coronary veins of hearts that were subjected to ischemia/reperfusion injury. Furthermore, while in other models, blockade of Mac-1 results in increases in rolling velocities of neutrophils, such treatment has the opposite effect in the heart (25, 33). These discrepancies could be due to tissue-specific molecular requirements for rolling versus anatomical or flow characteristics of coronary vessels.

Two subsets of monocytes have been identified in mice, $CX3CR1^{lo}Gr\text{-}1^{+}CCR2^{+}$ and $CX_3CR1^{hi}Gr\text{-}1^{-}CCR2^{-}$. $CX_3CR1^{hi}Gr\text{-}1^{-}CCR2^{-}$ monocytes are commonly referred to as "noninflammatory" or "resident." However, employing intravital microscopy, Auffray and colleagues observed that CX_3CR1^{hi} monocytes patrol peripheral tissues in the steady state and rapidly extravasate during inflammation (34). Once they enter inflamed tissues, they secrete proinflammatory cytokines to initiate innate immune responses. In this report, we show that CX_3CR1^{hi} cells are also rapidly recruited to hearts during ischemia/reperfusion injury. While these cells were far less numerous than neutrophils during our imaging period, they infiltrated heart grafts rapidly after reperfusion. Of note, a previous study showed that CX_3CR1 plays an important role in mediating monocyte recruitment to kidneys that are subjected to ischemia/reperfusion injury (35).

In conclusion, we have developed a technique to image beating hearts in vivo by 2P microscopy. This approach allows for the visualization of leukocyte behaviors within coronary arteries, veins, and myocardial tissue. Our results extend the notion that tissue-specific differences exist with regard to molecular requirements for leukocyte trafficking under inflammatory conditions. We suggest that intravital 2P imaging will provide a powerful tool for studying leukocyte trafficking and activation underlying various clinically relevant conditions such as formation of atherosclerotic plaques in the coronary arteries or infectious and autoimmune myocarditis.

Methods

Mice. B6 WT, B6 ICAM-1–mutant (B6.129S4-*Icam1*^{tm1Jcgr}/J), and B6 CX3CR1 GFP/GFP (B6.129P-*Cx3cr1*^{tm1Litt}/J) mice were purchased from The Jackson Laboratories. B6.129S4-*Icam1*^{tm1Jcgr}/J mice were generated by inserting the neomycin resistance gene into exon 4 of the *Icam1* gene. B6 CX_3CR1 GFP/GFP mice were bred with B6 mice to generate B6 CX_3CR1 GFP/+ mice. B6 LysM-GFP mice were obtained from Klaus Ley (La Jolla Institute for Allergy and Immunology, La Jolla, California, USA) and maintained at our facility.

Heart transplantation. Cardiac grafts harvested from WT B6 or B6 ICAM-1–mutant mice were transplanted into the right neck of B6 LysM-GFP recipient mice following 1 hour of cold (4°C) ischemia as previously described (36). Briefly, using cuff techniques, the recipient right common carotid artery and right external jugular vein were connected to the donor ascending aorta and the donor pulmonary artery, respectively. Upon reperfusion, grafts resumed a regular heartbeat. For select experiments, recipient mice were treated with either anti–LFA-1 (M17/4, BioXCell, NH), anti–Mac-1 (M1/70, BioXCell, NH) or control antibodies (100 μg intravenously 30 minutes before transplantation and 1 and 3 hours after transplantation.) 2P imaging was initiated 1 hour after implantation. The imaging procedure was terminal, and mice were euthanized while deeply anesthetized.

Flow cytometry. GFP^{hi} cells were analyzed in whole-blood and heart tissue that was digested in medium containing collagenase H and DNAse as previously described (8). Cells were first incubated with anti-mouse CD16/CD32 for 15 minutes at 4°C to block Fc receptors (Fcγ III/II receptor, 2.4G2; BD Biosciences — Pharmingen). Cells were stained with fluorochrome-labeled anti–Ly-6G (clone 1A8), anti–Gr-1 (clone RB6-8C5), or anti-CD115 (clone AFS98) antibodies or isotype controls (BD Biosciences — Pharmingen). Analysis was performed on a FACSCalibur (BD Bioscience) equipped for 4-color flow cytometry.

Histology. Hearts were fixed in formaldehyde, sectioned, and stained with H&E.

2P microscopy and data analysis. Time-lapse imaging was performed with a custom-built 2P microscope running ImageWarp acquisition software (A&B Software). Mice were anesthetized with an intraperitoneal injection of ketamine (50 mg/kg) and xylazine (10 mg/kg) and maintained with halved doses administered every hour. For native heart imaging, mice were intubated orotracheally with a 20-gauge angiocatheter and ventilated with room air at a rate of 120 breaths per minute and with a tidal volume of 0.5 ml. For time-lapse imaging of leukocyte migration in the tissue parenchyma, we averaged 15 video-rate frames (0.5 seconds per slice) during the acquisition to match the ventilator rate and minimize movement artifacts. 2P excitation produced a second harmonic signal from collagen within the myocardial tissue. Explanted hearts were imaged as previously described (8). Multidimensional rendering and manual cell tracking was done with Imaris (Bitplane). Data were transferred and plotted in GraphPad Prism 5.0 (Sun Microsystems Inc.) for creation of the graphs. The neutrophil cluster analysis was performed using the cluster analysis function of the T Cell Analysis Program (TCA) (John Dempster, University of Strathclyde, Glasgow, United Kingdom) using a 25-μm radius threshold for cell-to-cell distances (37).

Statistics. The unpaired 2-tailed Student's *t* test was used for statistical analysis. $P < 0.05$ was considered significant.

Study approval. All animal procedures were approved by the Animal Studies Committee at Washington University School of Medicine.

Acknowledgments

D. Kreisel and A.E. Gelman are supported by the National Heart, Lung and Blood Institute (1R01HL094601), and M.J. Miller is supported by the National Institute of Allergy and Infectious Diseases (AI077600) We thank Arlene Ligori for medical illustration.

Received for publication January 25, 2012, and accepted in revised form May 9, 2012.

Address correspondence to: Daniel Kreisel, Associate Professor of Surgery, Pathology and Immunology, Campus Box 8234, 660 South Euclid Avenue, Washington University in St. Louis, St. Louis, Missouri 63110-1013, USA. Phone: 314.362.6021; Fax: 314.367.8459; E-mail: kreiseld@wudosis.wustl.edu. Or to: Mark J. Miller, Assistant Professor of Pathology and Immunology, Campus Box 8118, 660 South Euclid Avenue, Washington University in St. Louis, St. Louis, Missouri 63110-1093, USA. Phone: 314.362.3044; Fax: 314.362.4096; E-mail: miller@pathology.wustl.edu.

1. McDonald B, et al. Intravascular danger signals guide neutrophils to sites of sterile inflammation. *Science*. 2010;330(6002):362–366.
2. Yang L, Froio RM, Sciuto TE, Dvorak AM, Alon R, Luscinskas FW. ICAM-1 regulates neutrophil adhesion and transcellular migration of TNF-alpha-activated vascular endothelium under flow. *Blood*. 2005;106(2):584–592.
3. Cinamon G, Shinder V, Alon R. Shear forces promote lymphocyte migration across vascular endothelium bearing apical chemokines. *Nat Immunol*. 2001;2(6):515–522.
4. Shulman Z, et al. Lymphocyte crawling and transendothelial migration require chemokine triggering of high-affinity LFA-1 integrin. *Immunity*. 2009;30(3):384–396.
5. Petri B, Phillipson M, Kubes P. The physiology of leukocyte recruitment: an in vivo perspective. *J Immunol*. 2008;180(10):6439–6446.
6. Vinten-Johansen J. Involvement of neutrophils in the pathogenesis of lethal myocardial reperfusion injury. *Cardiovasc Res*. 2004;61(3):481–497.
7. Jones SP, et al. Leukocyte and endothelial cell adhesion molecules in a chronic murine model of myocardial reperfusion injury. *Am J Physiol Heart Circ Physiol*. 2000;279(5):H2196–H2201.
8. Kreisel D, et al. In vivo two-photon imaging reveals monocyte-dependent neutrophil extravasation during pulmonary inflammation. *Proc Natl Acad Sci U S A*. 2010;107(42):18073–18078.
9. Jung S, et al. Analysis of fractalkine receptor CX(3) CR1 function by targeted deletion and green fluorescent protein reporter gene insertion. *Mol Cell Biol*. 2000;20(11):4106–4114.
10. Tsui BM, Kraitchman DL. Recent advances in small-animal cardiovascular imaging. *J Nucl Med*. 2009;50(5):667–670.
11. Cahalan MD, Parker I, Wei SH, Miller MJ. Two-photon tissue imaging: seeing the immune system in a fresh light. *Nat Rev Immunol*. 2002;2(11):872–880.
12. Miller MJ, Wei SH, Parker I, Cahalan MD. Two-photon imaging of lymphocyte motility and antigen response in intact lymph node. *Science*. 2002;296(5574):1869–1873.
13. Looney MR, Thornton EE, Sen D, Lamm WJ, Glenny RW, Krummel MF. Stabilized imaging of immune surveillance in the mouse lung. *Nat Methods*. 2011;8(1):91–96.
14. Chalasani G, et al. The allograft defines the type of rejection (acute versus chronic) in the face of an established effector immune response. *J Immunol*. 2004;172(12):7813–7820.
15. Romson JL, Hook BG, Kunkel SL, Abrams GD, Schork MA, Lucchesi BR. Reduction of the extent of ischemic myocardial injury by neutrophil depletion in the dog. *Circulation*. 1983;67(5):1016–1023.
16. Litt MR, Jeremy RW, Weisman HF, Winkelstein JA, Becker LC. Neutrophil depletion limited to reperfusion reduces myocardial infarct size after 90 minutes of ischemia. Evidence for neutrophil-mediated reperfusion injury. *Circulation*. 1989;80(6):1816–1827.
17. Zarbock A, Singbartl K, Ley K. Complete reversal of acid-induced acute lung injury by blocking of platelet-neutrophil aggregation. *J Clin Invest*. 2006;116(12):3211–3219.
18. Kornerup KN, Salmon GP, Pitchford SC, Liu WL, Page CP. Circulating platelet-neutrophil complexes are important for subsequent neutrophil activation and migration. *J Appl Physiol*. 2010;109(3):758–767.
19. Patrick AL, Rullo J, Beaudin S, Liaw P, Fox-Robichaud AE. Hepatic leukocyte recruitment in response to time-limited expression of TNF-alpha and IL-1beta. *Am J Physiol Gastrointest Liver Physiol*. 2007;293(4):G663–672.
20. Jaeschke H, Farhood A, Fisher MA, Smith CW. Sequestration of neutrophils in the hepatic vasculature during endotoxemia is independent of beta 2 integrins and intercellular adhesion molecule-1. *Shock*. 1996;6(5):351–356.
21. Kukielka GL, et al. Regulation of intercellular adhesion molecule-1 (ICAM-1) in ischemic and reperfused canine myocardium. *J Clin Invest*. 1993;92(3):1504–1516.
22. Yamazaki T, et al. Expression of intercellular adhesion molecule-1 in rat heart with ischemia/reperfusion and limitation of infarct size by treatment with antibodies against cell adhesion molecules. *Am J Pathol*. 1993;143(2):410–418.
23. Palazzo AJ, Jones SP, Girod WG, Anderson DC, Granger DN, Lefer DJ. Myocardial ischemia-reperfusion injury in CD18- and ICAM-1-deficient mice. *Am J Physiol*. 1998;275(6 pt 2):H2300–H2307.
24. Poston RS, Ing DJ, Ennen MP, Hoyt EG, Robbins RC. ICAM-1 affects reperfusion injury and graft function after cardiac transplantation. *J Surg Res*. 1999;87(1):25–31.
25. Phillipson M, Heit B, Colarusso P, Liu L, Ballantyne CM, Kubes P. Intraluminal crawling of neutrophils to emigration sites: a molecularly distinct process from adhesion in the recruitment cascade. *J Exp Med*. 2006;203(12):2569–2575.
26. Carman CV, Springer TA. A transmigratory cup in leukocyte diapedesis both through individual vascular endothelial cells and between them. *J Cell Biol*. 2004;167(2):377–388.
27. Shaw SK, et al. Coordinated redistribution of leukocyte LFA-1 and endothelial cell ICAM-1 accompany neutrophil transmigration. *J Exp Med*. 2004;200(12):1571–1580.
28. Bowden RA, et al. Role of alpha4 integrin and VCAM-1 in CD18-independent neutrophil migration across mouse cardiac endothelium. *Circ Res*. 2002;90(5):562–569.
29. Ding ZM, et al. Relative contribution of LFA-1 and Mac-1 to neutrophil adhesion and migration. *J Immunol*. 1999;163(9):5029–5038.
30. Niessen HW, Lagrand WK, Visser CA, Meijer CJ, Hack CE. Upregulation of ICAM-1 on cardiomyocytes in jeopardized human myocardium during infarction. *Cardiovasc Res*. 1999;41(3):603–610.
31. Entman ML, et al. Neutrophil induced oxidative injury of cardiac myocytes. A compartmented system requiring CD11b/CD18-ICAM-1 adherence. *J Clin Invest*. 1992;90(4):1335–1345.
32. Henderson RB, et al. The use of lymphocyte function-associated antigen (LFA)-1-deficient mice to determine the role of LFA-1, Mac-1, and alpha4 integrin in the inflammatory response of neutrophils. *J Exp Med*. 2001;194(2):219–226.
33. Dunne JL, Ballantyne CM, Beaudet AL, Ley K. Control of leukocyte rolling velocity in TNF-alpha-induced inflammation by LFA-1 and Mac-1. *Blood*. 2002;99(1):336–341.
34. Auffray C, et al. Monitoring of blood vessels and tissues by a population of monocytes with patrolling behavior. *Science*. 2007;317(5838):666–670.
35. Li L, et al. The chemokine receptors CCR2 and CX3CR1 mediate monocyte/macrophage trafficking in kidney ischemia-reperfusion injury. *Kidney Int*. 2008;74(12):1526–1537.
36. Matsuura A, Abe T, Yasuura K. Simplified mouse cervical heart transplantation using a cuff technique. *Transplantation*. 1991;51(4):896–898.
37. Gelman AE, et al. Cutting edge: Acute lung allograft rejection is independent of secondary lymphoid organs. *J Immunol*. 2009;182(7):3969–3973.